The Axonemal Axis and Ca^{2+}-induced Asymmetry of Active Microtubule Sliding in Sea Urchin Sperm Tails

Winfield S. Sale

Department of Anatomy and Cell Biology, Emory University School of Medicine, Atlanta, Georgia 30322

Abstract. Structural studies of stationary principal bends and of definitive patterns of spontaneous microtubule sliding disruption permitted description of the bending axis in sea urchin sperm tail axonemes. *Lytechinus pictus* sperm were demembranated in a buffer containing Triton X-100 and EGTA. Subsequent resuspension in a reactivation buffer containing 0.4 mM $CaCl_2$ and 1.0 mM $MgATP^{2-}$ resulted in quiescent, rather than motile, cells and each sperm tail axoneme took on an extreme, basal principal bend of 5.2 rad. Thereafter, such flagellar axonemes began to disrupt spontaneously into two subsets of microtubules by active sliding requiring ATP. Darkfield light microscopy demonstrated that subset "1" is composed of microtubules from the inside edge of the principal bend. Subset "2" is composed of microtubules from the outside edge of the principal bend and always scatters less light in darkfield than subset 1. Subset 2, which always slides in the proximal direction, relative to subset 1, results in a basal loop of microtubules, and the subset 2 loop is restricted to the bend plane during sliding disruption. Electron microscopy revealed that doublets 8, 9, 1, 2, 3 and the central pair comprise subset 1, and doublets 4, 5, the bridge, 6, and 7 comprise subset 2. The microtubules of isolated subset 2 are maintained in a circular arc in the absence of spoke–central pair interaction. Longitudinal sections show that the bending plane bisects the central pair. We therefore conclude that the bend plane passes through doublet 1 and the 5-6 bridge and that doublet 1 is at the inside edge of the principal bend. Experimental definition of the axis permits explicit discussion of the location of active axonemal components which result in Ca^{2+}-induced stationary basal bends and explicit description of components responsible for alternating basal principal and reverse bends.

We began these studies to investigate a radial "switching" model for regulation of active microtubule sliding in the formation of alternating basal bends in cilia and eukaryotic flagella (for review see reference 39). The hypothesis is that alternating principal and reverse basal bends are caused by the alternate activation of active microtubule sliding on opposite sides of the axoneme (40, 45, 47). This proposal is a consequence, in part, of the radial symmetry of dynein arms around ciliary and flagellar 9 + 2 axonemes and of the belief that the force generation of all dynein arms is unidirectional (37). Although the hypothesis is an oversimplification of the complexity of both radial and longitudinal patterns of active microtubule sliding that can be predicted for steady state bending waves in flagellar axonemes (18, 20–22, 44), it is a useful model in analysis of regulation of patterns of active microtubule sliding in the formation of basal bends and in analysis of modulated patterns of microtubule sliding in Ca^{2+}-modified waveforms (2, 6, 8, 12, 18, 21, 39). However, patterns of active microtubule sliding can be discussed in precise relationship to axonemal structures only if the axonemal axis is defined relative to the bending axis and bending direction.

Structural asymmetry, based upon the "5-6 bridge" and the central pair, has long been recognized for the axoneme in sea urchin sperm tails (1, 14, 15). This asymmetry in structure is the original basis for numbering doublet microtubules in this axoneme, but the axis of the axoneme in relationship to the bending plane and direction has not been determined. Rather, in the absence of data it has been assumed that the axis in the axoneme of the sea urchin sperm tail is the same as that in epithelial cilia which contain a 5-6 bridge and in which the axonemal axis, bending plane, and bending direction had been correlated (13, 38). Considering the prominent role the sea urchin sperm cell continues to play in experimental determination of the mechanism of regulation of microtubule sliding in the formation of normal bending waves of the axoneme (3, 4, 17, 22, 42) and in determination of the mechanisms of calcium-induced modulation of normal bending (2, 8, 9, 11, 12, 18, 19, 27–29), it is important that the structural axis of this axoneme be precisely defined in relationship to the bending axis.

In the work reported here we have taken advantage of both structural markers in the axoneme of the sea urchin sperm tail and properties of the spontaneous, planar pattern of Ca^{2+}- and ATP-induced sliding disruption of the axoneme to (*a*) determine the axonemal axis with respect to the bending axis

of the flagellum, and (*b*) investigate the capability of the axoneme to restrict active sliding to one side of the axis in the formation of uniform, stationary basal bends. As assumed in earlier reports, we have found that the bending plane bisects the central pair and passes through doublets 1 and the 5-6 bridge, and that doublet 1 is located at the inside edge of the principal bend. A similar conclusion has been reached for the axis of the axoneme in starfish sperm (26). The patterns of axonemal fracture observed after spontaneous microtubule sliding are comparable to those described by Tamm and Tamm (45) in study of the sliding disintegration of the macrocilium from the ctenophore *Beroë* and to those described by Olsen and Linck (30) of the sliding disintegration of rat sperm axonemes. These data are generally consistent with a radial "switching model" of basal bend formation in which opposite sides of the axoneme are alternatively active in formation of principal and reverse bends (39, 40, 47). The results were presented at the 25th Annual Meeting of the American Society for Cell Biology (35).

Materials and Methods

Lytechinus pictus sperm were obtained by injection with KCl, and undiluted semen was stored on ice until used. All subsequent procedures were carried out at 19–20°C. In a few cases sperm from *Strongylocentrotus purpuratus* were used.

Demembranation and Reactivation

Our standard procedure for demembranation was to transfer 25 μl of concentrated sperm cells to 0.5 ml of a demembranation buffer comprised of 10 mM Tris-base (pH 8.15), 0.15 M potassium acetate, 2 mM EGTA, 1 mM $MgSO_4$, 1 mM dithiothreitol, and 0.05% (wt/vol) Triton X-100. After 30 s, 25 μl of demembranated cells was diluted into 2.5 ml "reactivation" buffer contained in petri dishes constructed with 2 × 3-in. glass slides and pyrex rings (10). The standard reactivation buffer contained 10 mM Tris-base (pH 8.15), 0.15 M potassium acetate, 2 mM $MgSO_4$, 1 mM ATP, 1 mM dithiothreitol, 0.4 mM $CaCl_2$, and 0.1 mM EGTA. These conditions of demembranation and reactivation resulted in quiescent sperm with a characteristic extreme, basal principal bend (Fig. 1 *a* and see references 12 and 34). Variations in the concentration of Ca^{2+}, Mg^{2+}, ATP, or dithiothreitol in the reactivation buffer are described in Results. "Free" Ca^{2+}, Mg^{2+}, $MgATP^{2-}$, and $CaATP^{2-}$ were determined by computer program, and equilibrium constants were supplied by C. J. Brokaw (see reference 5).

Light Microscopy

Light microscopy was carried out using either a 100-W halogen or xenon strobe (Chadwick Helmuth Co., Inc., El Monte, CA) light source, green interference filter, Zeiss darkfield ultracondensor (1.2/1.4 numerical aperture), and a water immersion objective lens (either 25× or 40× Plan Neofluar immersion lens, Carl Zeiss, Inc., Thornwood, NY). Cells were studied in suspension near the slide surface. However, precautions were taken in the assessment of cells attached to the slide surface since attachment often induced random patterns of ATP-induced sliding disruption.

For photomicroscopy, Tri-X film was exposed by single or multiple flashes of the xenon strobe and developed at 34°C in Diafine developer (Acufine, Inc., Chicago, IL). Video recordings made use of an MTI camera equipped with a newvicon tube or an MTI S.I.T.-66 camera (DAGE-MTI, Inc., Wabash, MI). Recordings were on ½-in. video tape on the Panasonic NV 8050 time lapse recorder, and noise-free field by field analysis of motility was carried out with a Panasonic NV 8950 recorder (Panasonic Co., Secaucus, NY). In some cases image contrast from video recordings was enhanced using the Hughes Model 794 image processor (Hughes Aircraft Co., El Segundo, CA). Cell size, shape, and microtubule lengths were determined from tracings made directly from the video monitor at a final magnification of 3,000. (All size and length measurements listed in Table I were repeated from other experiments using prints made from 35-mm film to verify the accuracy of measurements made from the video monitor). Rates of sliding were determined from video recordings by timing the duration of sliding for measured averaged lengths of microtubule. Patterns of sliding disruption were determined by reconstruction from video recordings.

Electron Microscopy

Samples of demembranated cells were prepared for electron microscopy by diluting such a suspension with an equal volume of 2% glutaraldehyde made up in a buffer identical to that used for reactivation. After a 10-min incubation in fixative, cell samples were pelleted at 10,000 rpm for 15 min in the Sorvall HB-4 swinging bucket rotor (DuPont Co., Wilmington, DE). (To obtain pellets of convenient size, the standard number of cells and volume of reactivation buffer was scaled up fourfold). Thereafter, pellets were overlaid with 1% glutaraldehyde in 0.15 M sodium cacodylate buffer (pH 7.4), and fixed overnight. Samples were postfixed in 1% OsO_4 in cacodylate buffer, dehydrated in a graded ethanol series, and embedded in Epon-araldite. Uniform silver-grey sections were collected on formvar-coated, carbon-stabilized copper grids, and stained with uranyl acetate and lead citrate. Photomicrographs of cross-sections were taken by an unbiased investigator, and micrographs of the cross-sections were analyzed and scored by two different observers unaware of the sample treatment before fixation.

Breakage Assay

We developed a light microscopic assay for rapid, reproducible measurement of the degree of integrity of sperm tail axonemes vs. the degree of ATP-induced sliding disruption. This was necessary to facilitate large numbers of measurements for the variety of reactivation buffer conditions displayed in Table II and Fig. 4. Demembranated cells were suspended as usual in petri dishes containing reactivation buffer of prescribed composition. After incubation for a predetermined length of time, the dishes were gently flooded with an equal volume of 2% glutaraldehyde in a buffer identical in composition to the reactivation buffer. After 5-min fixation, aliquots of the supernate were transferred to a slide and a coverslip was then added. Using the ultracondensor and a Zeiss 25× Plan Apochromatic objective lens, 100 randomly selected cells were scored as "intact" (as in Fig. 1 *a* or Fig. 1 *b*) or "broken" (as in Fig. 1, *c–f*). Each cell counted was carefully observed in three dimensions by fine focusing to be certain of the integrity of the axoneme. Cells were rarely damaged and distorted by adhesion to the substrate after fixation. Nevertheless, headless axonemes, transversely fractured axonemes, and excessively splayed axonemes were sometimes found and were not counted. Otherwise, all cells in each field were included in counts. Counts were carried out by two individuals who were unaware of sample treatment before fixation, and all experiments were repeated at least four times. Data are displayed as the mean percentage broken. The assay is convenient and reproducible and the degree of breakage is comparable to that found by electron microscopic analyses of similarly treated samples.

Materials

Deionized water was used throughout. ATP was purchased from Boehringer Mannheim Diagnostics, Inc. (Houston, TX). Sodium metavanadate and potassium acetate were from Fisher Scientific Co. (Pittsburgh, PA). Elastase was from Calbiochem-Behring Corp. (La Jolla, CA). Tris-base, EGTA, $CaCl_2$, $MgSO_4$, and dithiothreitol were from Sigma Chemical Co. (St. Louis, MO).

Results

Characterization of Stationary Principal Bends and the Spontaneous Microtubule Sliding Disruption

When sperm from *L. pictus* are demembranated and reactivated by the standard conditions described in Materials and Methods the cells become quiescent and take on uniform basal principal bends (Fig. 1 *a*). The principal bend has an average angle of 5.19 rad and a radius of curvature of ~1.7 μm (Table I). The distal axoneme has a slight reverse bend midway along the axoneme which gradually, over 1–5 min, increases in bend angle (*iii*, Fig. 1 *b*). The generation of the basal principal bend requires Ca^{2+} and ATP and can be relaxed by micromolar vanadate as reported earlier (12, 34).

After incubation of ~5 min, the sperm tail axonemes begin to break into two subsets of microtubules by sliding disruption (*1* and *2*, Fig. 1). Results of such disruption are illustrated in Fig. 1, *c–f*, in which active sliding leads to partial separation of axonemes into subset 1 from the inside edge of the principal bend and subset 2, which slides from the periphery or outside

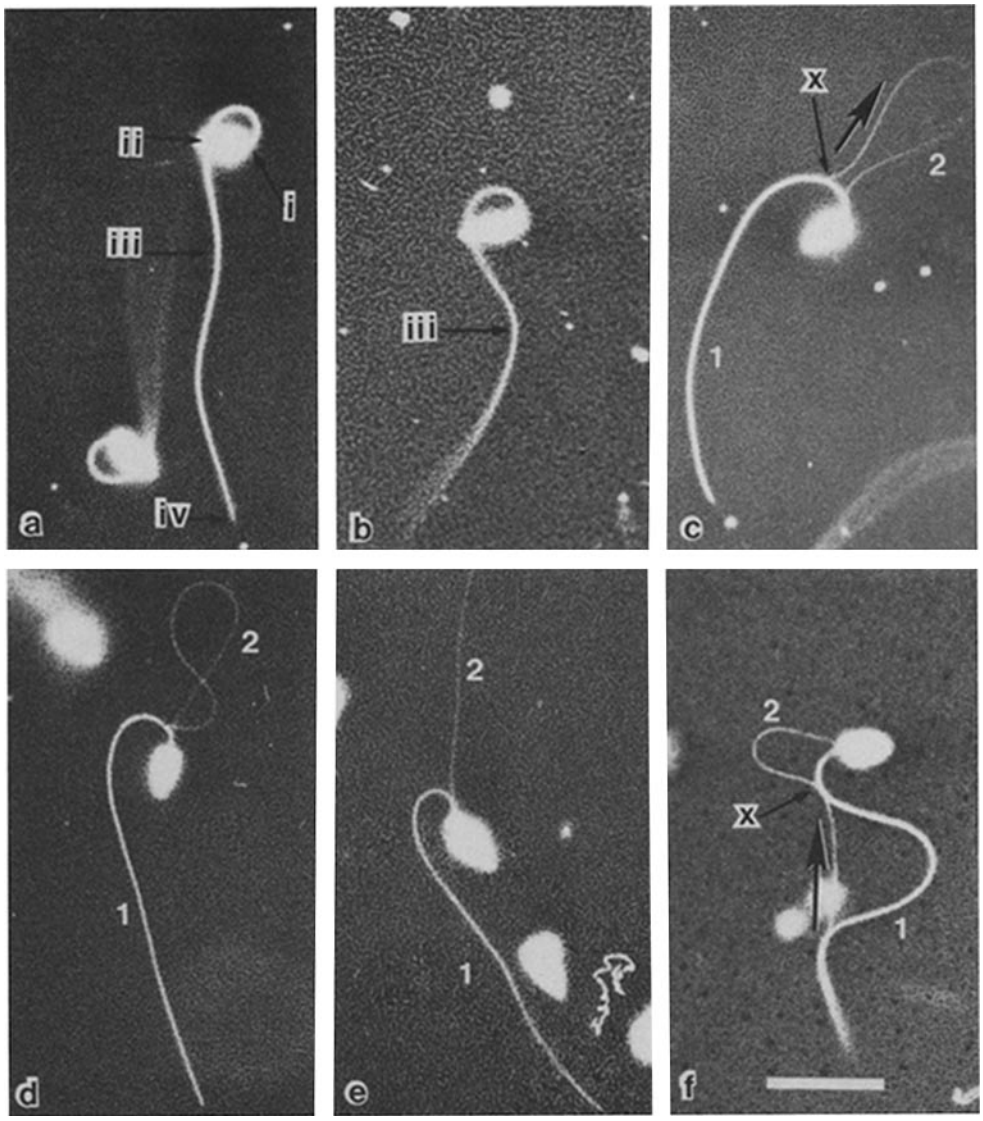

Figure 1. Darkfield light micrographs of demembranated sperm (*L. pictus*) cells suspended in the standard reactivation buffer. *a* is the characteristic shape of the Ca^{2+}- and ATP-induced quiescent sea urchin sperm with a sharp basal principal bend and a relatively gentle reverse bend (*iii* in *a*) midway along the axoneme. After incubation the reverse bend increases in angle as illustrated in *b*. After ~5 min (see time course Fig. 4) many of the sperm tails begin to break into two microtubule subsets (*1* and *2*, in *c–f*) by active sliding. Subset *2*, which scatters less light in darkfield, slides out from site *x* on the outside edge of the principal bend (*c* and *f*) and always slides in the proximal direction relative to subset 1. The symbols *i*, *ii*, *iii*, and *iv* refer to the approximate locations of the basal body, distal end of the principal bend, center of the reverse bend, and axonemal distal tip. The pattern of disruption is illustrated in Fig. 2. Bar, 10 μm.

edge of the principal bend as a loop. Subset 2 always slides proximally (large arrow in Fig. 1, *c* and *f*) and scatters less light in darkfield relative to subset 1. Subsets 1 and 2 usually remain attached at both the basal body and more distally at site "x", an approximate point within the basal bend where subsets 1 and 2 initially separate.

From videotape recordings we have reconstructed several features of the process and pattern of the spontaneous sliding disruption of the axoneme. Sequences of the two typical patterns are shown in Fig. 2. Sliding disruption is preceded by an increase in the angle of the reverse bend as described above (Fig. 1 *b*). This increase in angle lasts for various lengths of time before disruption. Initiation of sliding of subset 2 is immediately preceded by a "twitch" of the axoneme in which the angle of the principal bend fleetingly and slightly increases and correspondingly the reverse bend straightens (Fig. 2 *a*, sequence *:39[5]* to *:40[4]*). Subset 2 then begins to slide and separates from subset 1 at site x: about mid-length along the arc of the principal bend (see Table I). Subset 2 slides at ~12 μm/s forming a loop (curved arrows, Fig. 2). The remaining principal bend relaxes during transit of subset 2 resulting in the C-shaped arc of subset 1 bent in the principal bend direction (Figs. 1 *c* and 2 *a*). The loop formed by subset 2 averaged 35 μm, whereas the axoneme averaged 40 μm (Table I): thus the subsets overlap by ~5 μm after movement. The subset 2 loop often became twisted after sliding (Fig. 1 *d*), or slid entirely off subset 1 and straightened (Fig. 1 *e*). Importantly, edge-on or end-on views revealed that subset 2 slides in the same plane as the principal bend during transit. Attachment of sperm tail axonemes to the slide surface often resulted in unrestricted sliding disruption of the axonemes, as illustrated in Fig. 3.

In many examples spontaneous sliding was accompanied by an apparent firm attachment of subsets 1 and 2 at the distal end of the axoneme (Figs. 1 *f* and 2 *b*). In such cases, subset 2 slides proximally forming a loop at site x as usual but concomitantly compresses subset 1, in "accordion fashion," at the principal and reverse bends (Fig. 2 *b*). In these cases sliding also remains restricted to the bending plane, and the shear forces required for sliding are presumably restricted to the contact region just distal to site x. We have recorded several cases of this form of sliding disruption in which subsets

1 and 2 remain fused distally, but then, after proximal sliding, separate at site x. In such cases the axoneme elastically straightens after separation of subsets 1 and 2 at site x and then apparently re-anneal and the axoneme repeatedly undergoes the identical pattern of unipolar sliding each time recompressing the axoneme at the principal and reverse bends. In such repetitive sliding events, the relative polarity of active sliding between subsets 1 and 2 is maintained: under our standard conditions we have never witnessed subset 2 actively slide in the distal direction relative to subset 1 (≫1,000 examples observed).

The same patterns of disruption take place in sperm tails without heads. However, it appears that the basal body is necessary since the principal bend and breakage of headless tails require full length axonemes with a distinct bright "dot" at the proximal end of the axoneme as determined by dark-field light microscopy. We interpret the dot as the basal body and associated cellular structures.

*Table I. Cell Size and Shape and Motility Parameters of Restricted, Spontaneous Sliding Disruption**

		n
Axoneme length (*i–iv*, Fig. 1 *a*)	40.0 ± 2.1 μm	66
Principal bend		
Angle	5.19 ± 0.4 rad	25
Radius of curvature	1.7 ± 0.3 μm	27
Arc length (measured) (*i–ii*, Fig. 1 *a*)	6.9 ± 1.2 μm	43
Distance, basal body to site × (i–x, Fig. 1 *a*)	3.8 ± 1.6 μm	44
Distance, basal body to midpoint of reverse bend (*i–iii*, Fig. 1 *a*)	19.3 ± 2.5 μm	33
Length subset 2	35.0 ± 4.5 μm	23
Rate of sliding‡	11.93 μm/s	10

* All length and angle measurements made on traces taken from a video screen. Measurements were made at 3,000×. Length segments (*i–ii*, etc.) are defined in Fig. 1 *a*.

‡ Sliding rates were measured with a stop watch from video recordings. Sliding rate was calculated by dividing average loop length by average total time for sliding.

Factors That Affect the Degree of Spontaneous Axonemal Sliding Disruption

Using the breakage assay described in Materials and Methods, we studied the time course and factors that affect the restricted pattern of breakage of the sperm tail axonemes. Under standard conditions breakage begins at ~5 min and reaches a plateau at ~15 min of 60–70% of the axonemes which undergo active sliding disruption (Fig. 4; Table II). Thereafter, there is no significant increase in spontaneous sliding breakage. Therefore, 16 min was chosen as the stop point to test buffer conditions and other factors that affect the pattern or extent of sliding disruption.

Breakage requires that the reactivation buffer contain ATP, dithiothreitol, and Ca^{2+} (Table II). Without anyone of these ingredients the axonemes remain intact. Addition of 0.4 mM EGTA or reduction of added Ca^{2+} to 0.1 mM also inhibited breakage. Interestingly, deletion of Mg^{2+} and the addition of 0.1 mM EDTA (to chelate Mg^{2+} transferred from the seawater) had no effect on the extent of ATP-induced sliding disruption. Furthermore, the removal of Mg^{2+} resulted in no apparent difference from the controls in the form of sliding disruption as revealed by direct observation and by video recordings. This suggested that $CaATP^{2-}$ can support the spontaneous sliding separation of subsets 1 and 2. Reduction of ATP to 50 μM resulted in an increase of intact axonemes,

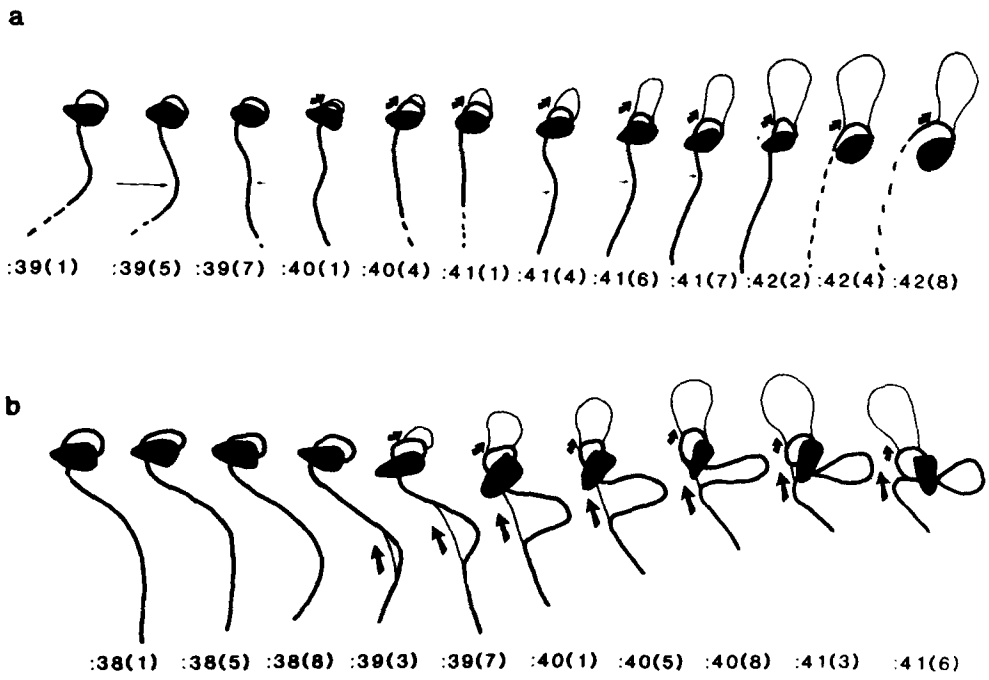

Figure 2. Traces from frames of video recordings of two predominant patterns of active disruption of the axoneme into subsets 1 and 2. Time is in seconds followed in parentheses by successive field advances which are ~0.13 s apart. The thick, curved arrows point in the direction of sliding of subset 2. *a* illustrates the most common pattern of breakage in which subset 2 begins to loop out at time *:40(1)*. Subset 2 remains restricted to the bending plane during sliding. *b* illustrates another pattern of breakage in which the two microtubule subsets apparently remain firmly attached to each other at the distal end of the axoneme as well as at site x and basal body. In all cases observed, subset 2 slides in the proximal direction only, and sliding is planar throughout as determined by edge on or end on views or determined by optical sections of side views. The dashed lines are segments that are tilted slightly out of focus.

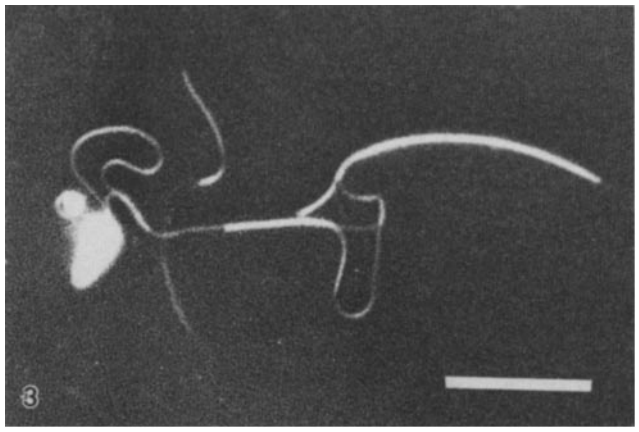

Figure 3. Darkfield light microscopy reveals that the absorption of sperm tail axonemes or doublet subsets 1 and 2 to the slide surface can induce further unrestricted patterns of sliding disruption. Fig. 3 displays one such example in which subset 1 has disrupted on the slide into several smaller groups of doublet microtubules. It is important to note that continued disruption of adherent axonemes is by a sliding mechanism and not by random fractures or fraying of the axoneme. Bar, 10 μm.

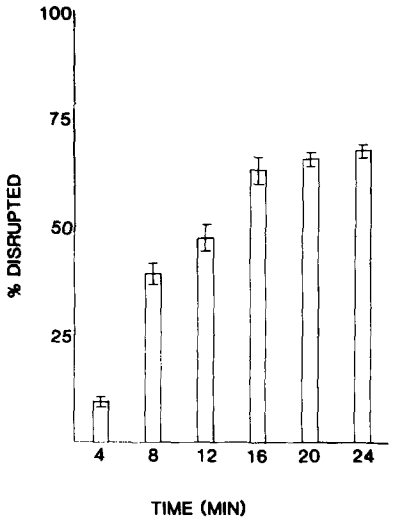

Figure 4. Time course of active sliding disruption of the entire population of demembranated cells determined by darkfield light microscopy using the "breakage assay". Data are plotted as the mean percent broken and bars are SEM. A plateau of spontaneous breakage is reached in ~15 min. Breakage is strictly defined as the limited patterns of disruption illustrated in Fig. 1, *c–f*. There is close correspondence for the percentage of fractured axonemes between the breakage assay and electron microscopy of cross-sections.

as revealed by the breakage assays, and such reduced concentrations of ATP resulted in renewed motility rather than quiescence as described earlier (4, 12, 34).

The potential role of proteases in breakage was examined. Soybean trypsin inhibitor, antipapain, and leupeptin (at 25 and 50 μg/ml) had no effect on the form or extent of breakage under standard conditions. However, 25 or 50 μg/ml of chick ovoinhibitor (Sigma T 1886) reduced breakage to 30% of control levels. This result suggested that an elastase-like protease may help provide for sliding disruption (3, 45).

For suspended sperm tail axonemes in the standard reacti-

Table II. Comparison of the Light Microscopic "Breakage Assay" with Electron Microscopic Analysis of Axonemal Fracture by Sliding Disruption

Time course*	Breakage assay	Electron microscopy‡
Spontaneous disruption	% Broken (*n*)	% Broken (*n*)
min		
4	18 (100)	14 (82)
8	20 (105)	17 (142)
12	42 (100)	34 (130)
16	56 (96)	49 (98)
Effects of changes in standard buffers	Breakage assay	Electron microscopy
	% Broken§	% Broken (*n*)
Control (standard buffers)	60 ± 2	50 (180)
$-Ca^{++}$	9 ± 1.8	0 (246)
+0.5 mM EGTA	13 ± 2.0	—
−ATP	1 ± 0.0	2 (282)
−Dithiothreitol	11 ± 3.1	—
$-Mg^{2+}$, + 0.1 mM EDTA	60 ± 1.0	—
+5 μM vanadate	0 ± 0	0 (350)

* Comparative light microscopic and electron microscopic time course data from identical samples in a single experiment. See Fig. 4 for average data from other time course experiments.

‡ Only axonemal profiles containing central pair were counted in order that broken axonemes were not counted twice. *n*, total number of axonemes counted.

§ Mean percentage broken (± SEM) from at least four different experiments.

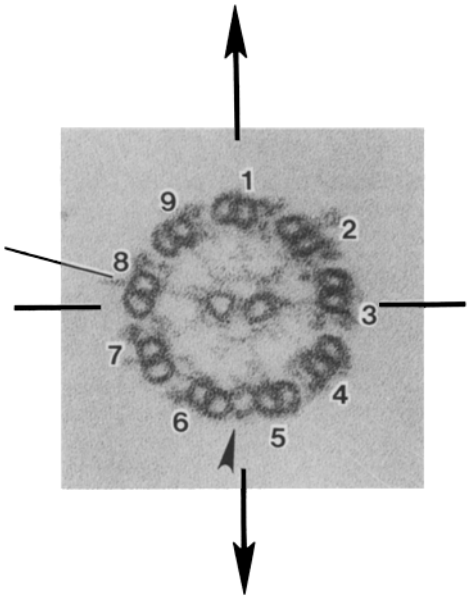

Figure 5. Standard cross-section of the sea urchin sperm tail axoneme viewed from base to tip. The central pair maintains a constant orientation relative to the 5-6 bridge, and therefore to other doublets numbered according to convention. The spoke of doublet 3 always sits in the plane which can be constructed through the central pair (*thick bars*) and the spoke of doublet 8 is rotated ~20° clockwise from this plane. The spoke of doublet 1 nearly bisects the central pair. All of these structural features impart asymmetric structure to the axoneme. The arrows suggest the beating plane deduced from other ciliary systems and as demonstrated below.

vation buffer containing 1 mM $MgATP^{2-}$, addition of elastase (8 or 16 μg/ml) promoted sliding disruption but did not change the pattern of sliding disruption described above or induce further unrestricted sliding of microtubules in subsets

1 and 2. However, microtubules of each subset will undergo further random unrestricted sliding disruption as illustrated in Fig. 3 if they become attached to the slide surface. Evidently restriction of sliding microtubules in subsets 1 and 2 can be overcome by the mechanical perturbation of adhesion. This result suggested that the restriction of sliding of doublets in subset 1 or 2 even after elastase treatment is not due to permanent impairment of dynein. At lowered $MgATP^{2-}$ (5–50 μM), addition of elastase resulted in random, unrestricted disruption (similar to that illustrated in Fig. 3) of both suspended sperm tails and those stuck to the surface.

Electron Microscopy of Demembranated Sea Urchin Sperm Cells

Cross-sections of sea urchin sperm tails confirm that the 5-6 bridge has a constant structural relationship to the central pair and therefore a constant relationship to all doublets (Fig. 5). Based upon study of stereo pair micrographs of replicas of quick-frozen, demembranated sea urchin sperm tails, we also confirmed that the dynein arms are oriented in a clockwise direction when cross-sections are viewed from the basal body toward axonemal tip (data not shown; see references 15 and 36). Other notable structural features of cross-sections are described in the legend of Fig. 5.

Longitudinal sections of the basal principal bend of quiescent demembranated sperm cells have revealed new details of the sperm head–tail attachment. The basal body terminates proximally in a dense staining cap-like structure (large arrow, Fig. 6) which, when viewed in the plane of the bend, is asymmetrically disposed and is skewed toward the inside of the principal bend. The basal body is connected to the sperm head by a prominent stamen-like array of filaments (small black-on-white arrowhead, Fig. 6*a*). The basal body may also be connected to the sperm head by a less prominent collar of filaments. The region of the basal body–axoneme transition contains a plate-like structure (thin arrow, Fig. 6*a*) and an amorphic "necklace" of material presumed to be remnants of mitochondrial and plasma membrane attachments to the axoneme.

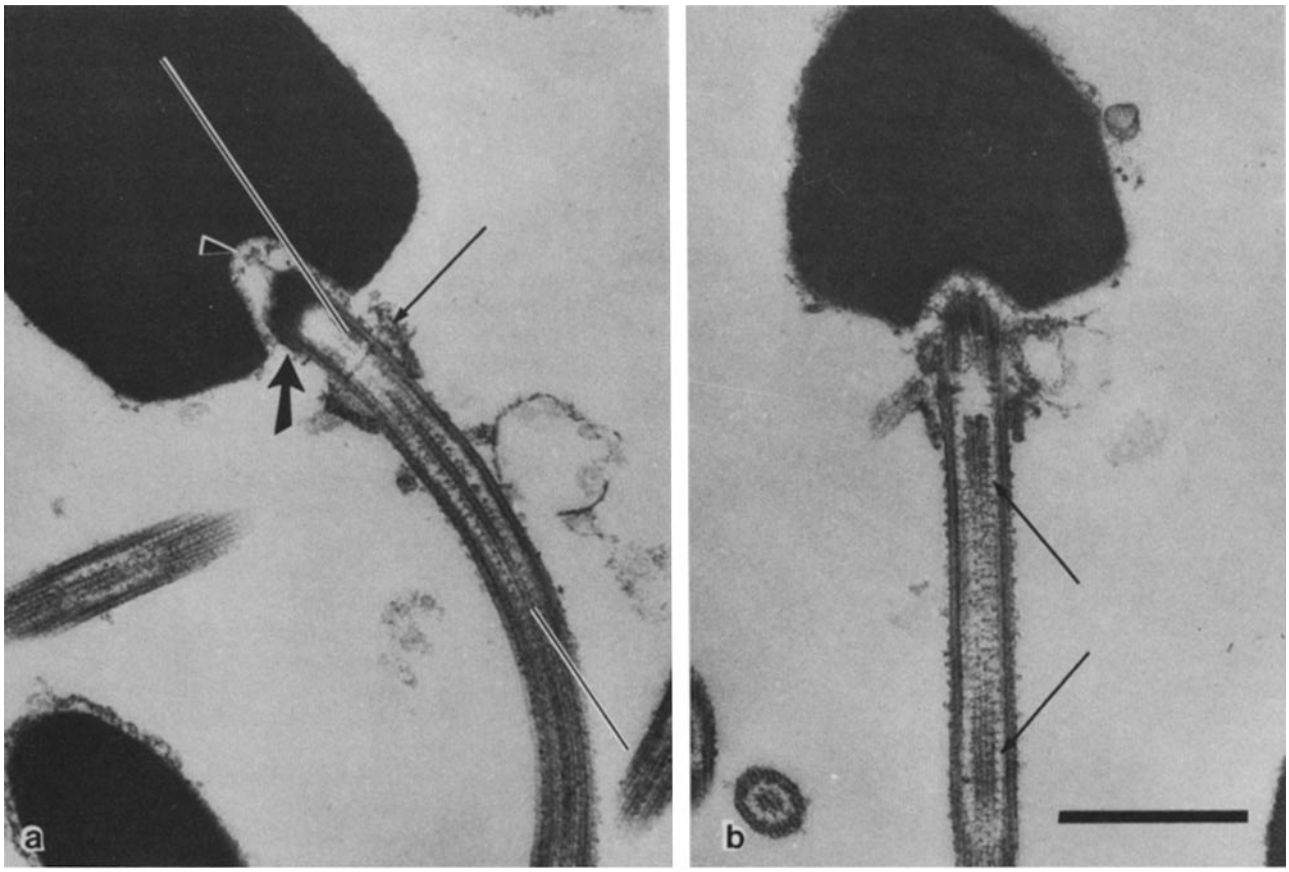

Figure 6. Longitudinal sections of glutaraldehyde fixed, nondisrupted stationary principal bends (produced in the absence of calcium as described in reference 34). The plane which can be artificially constructed through the central microtubule pair is always perpendicular to the plane of bend. This is illustrated in *a* in which a profile of a single central microtubule is located midway in such longitudinal views. *b* is a longitudinal section passing tangentially to the bend and perpendicular to that of *a* (approximately in the plane described by the thin lines of *a*). As predicted, such orientations reveal the central pair in parallel (*arrows* in *b*). Notably the dense staining proximal end of the basal body (*large arrow*) is attached to the head by a prominent, stamen-like structure (*arrowhead* in *a*). The same prominent, stamen-like connection is seen in intact, nondemembranated sperm cells from both *L. pictus* and *S. purpuratus* whether prepared by conventional fixation procedures described in Materials and Methods or by quick freeze and freeze substitution methods (data not shown). Based upon serial section reconstruction of three axonemes, in longitudinal view, we have no evidence for twist of either the central pair or doublet microtubules in the region of the bend. Bar, 0.5 μm.

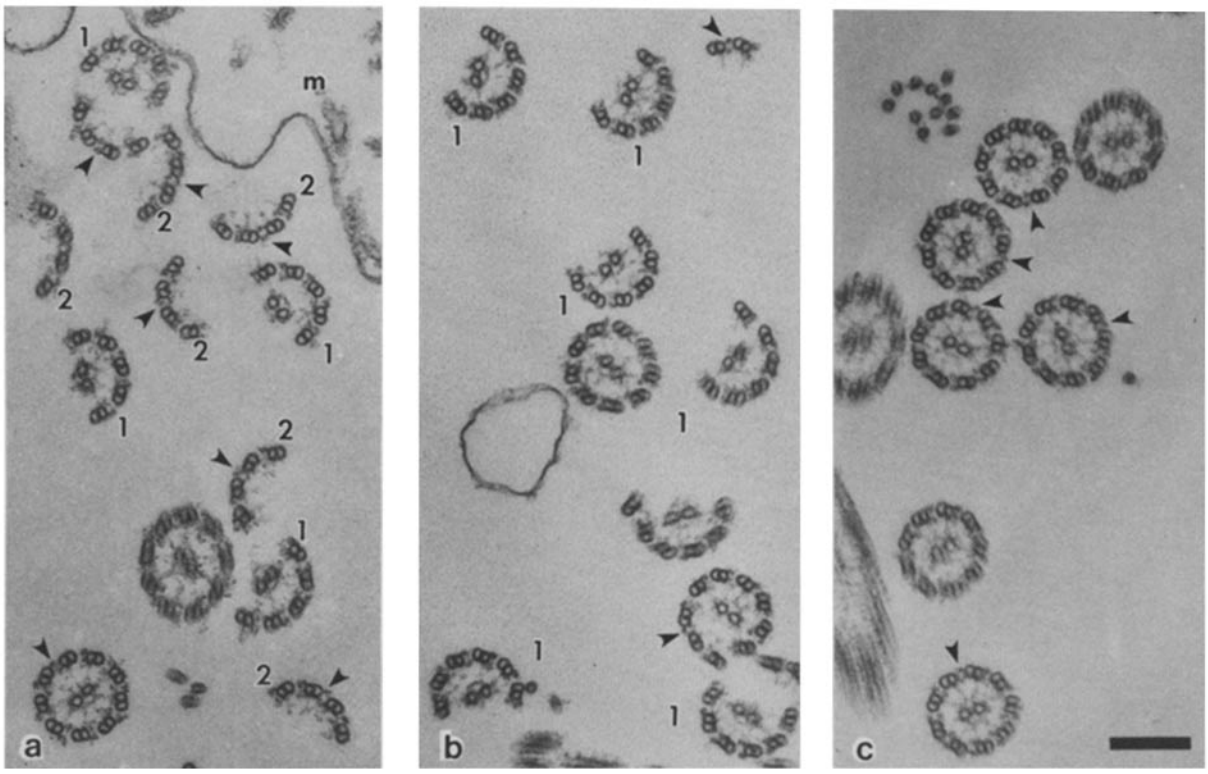

Figure 7. Exemplary micrographs of samples used in quantitative analysis (Table III) of the pattern of axonemal fracture after sliding disruption. Micrographs were selected to show large numbers of cross-sections of axonemes. A portion of a disrupted mitochondria (*m*) is also revealed. *a* is from a pellet of *L. pictus* sperm suspended in the base reactivation buffer and fixed in suspension before centrifugation. Axonemes are either intact or broken into two complementary subsets of microtubules: subset 1 usually contains doublets 8-3 plus the central pair and subset 2 contains doublet 4-7 and the 5-6 bridge (*arrowheads*). Subset 1 often contained doublets 8-4 (see Table III). *b* is a pellet of demembranated, elastase-treated (8 μg/ml) sperm (*S. purpuratus*) suspended in the standard reactivation buffer. In this case subset 1 is predominantly comprised of doublets 8-4 and the central pair (87%, $n = 132$ cross-sections, two experiments). Fig. 8*c* is a control sample of intact axonemes in which the reactivation buffer was devoid of calcium (*L. pictus*). A summary of frequencies and patterns of axonemal fracture is illustrated in Table III. Bar, 0.2 μm.

The central microtubule pair sit side by side in the plane of the bend. This is illustrated in Fig. 6*a* in which a mid-longitudinal section reveals the profile of only one of the central microtubules. Glancing longitudinal sections through bends and perpendicular to the plane of bend reveal paired central microtubules sitting side by side (Fig. 6*b*). In examples studied so far prepared by conventional glutaraldehyde fixation, there is no evidence of twisting of either the axoneme or the central pair in the region of the basal bend.

Microtubule Patterns in Subsets 1 and 2

There is close correspondence of the percentage of spontaneously disrupted axonemes as determined by the "breakage assay" and by electron microscopy of cross sections (Table II). The axonemes break into two complementary sets of microtubules: one set is usually comprised of doublets 8, 9, 1, 2, 3 and the central pair (*1*, Fig. 7*a*); a second complementary set is comprised of doublets 4, 5, the bridge, 6, and 7 (*2*, Fig. 7*a*). Deviations from this pattern of breakage were generally limited to shifts of one doublet number such that subset 1 contained doublets 7-4, 8-4, 9-4, or 9-3 and the central pair (patterns and frequencies shown in Table III and Scheme I). The frequency of patterns varied on occasion for unknown reasons (compare Exps. *1*, *2*, and *3* with Exp. *4* in Table III). Since subset 1 scatters the most light when viewed by dark-field, we conclude that it is comprised of doublets 8-3 and the central pair. This conclusion is confirmed by longitudinal sections in the plane of bend of fractured axonemes and in whole mounted, negative-stained axonemes in which the central pair remained with the microtubules on the inside edge of the principal bend (data not shown). The spokes remain attached to the doublet of origin after fracture, and the orientation of central pair and 5-6 bridge relative to doublet positions does not change (Fig. 7 and Scheme I). As described for the "breakage assay" electron microscopy revealed that Ca^{2+} and ATP were required for axonemal breakage, and vanadate-treated samples remained intact (Fig. 7*c*; Table II).

A restricted pattern of active sliding disruption similar to that described in Figs. 1 and 2 was found for the sperm of *S. purpuratus*. However, under standard reactivation conditions spontaneous breakage was less frequent. We therefore treated the *S. purpuratus* sperm with elastase (8 or 16 μg/ml) which resulted in rapid sliding disruption into subsets 1 and 2. In this case subset 1 was uniformly comprised of doublets 8, 9, 1, 2, 3, 4 and the central pair (Fig. 7*b*), and subset 2 was variable and comprised of one, two, or three doublets. Presumably variability in subset 2 was due to continued disruption in the presence of elastase and ATP.

Table III. Patterns and Frequency of Axonemal Fracture after Active Sliding Disruption

	L. pictus—spontaneous sliding disruption			
Exps. 1, 2, and 3*				
Subset 1	8-3	8-4	7-4‡	$n = 269$
	71%	18%	—	
Subset 2	4-7	5-7	5-6	$n = 109$
	76%	13%	11%	
Exp. 4				
Subset 1	8-3	8-4	7-4	$n = 89$
	29%	30%	42%	
Subset 2	4-7	5-7	5-6	$n = 38$
	26%	24%	50%	

* Experiments averaged because there was no significant difference in pattern frequency.

‡ A small percentage of 9-3 and 9-4 subset 1 patterns were also found. This suggests the active dynein arms of doublet 8 can induce proximal sliding of subset 2.

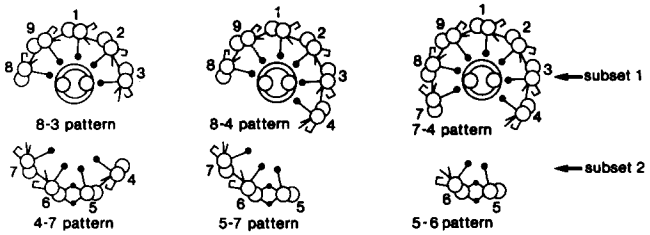

Scheme I. Most common patterns of axonemal fracture.

Discussion

The Axonemal Axis in Sea Urchin Sperm Tails

The results described here establish that the bending plane of sea urchin sperm tails bisects the central pair and passes through doublet 1 and the 5-6 bridge (Fig. 8). This conclusion is based upon longitudinal sections of basal bends parallel to the bend plane, upon longitudinal sections tangential to the bend and normal to the bend plane (Fig. 6), and upon the constant relationship of the central pair to the 5-6 bridge and therefore to the doublet microtubules (Figs. 5 and 8). Unlike the axonemes of certain cilia and flagella (24, 32), we provide no evidence for the rotation of the central pair or twist in the axoneme in the region of the basal bend for the sea urchin sperm tails. In structural studies of stationary bends in Ciona sperm tails, Omoto and Brokaw (31) also conclude there is no axonemal twist in the region of the bend. However, there is other evidence for axonemal twist associated with bends in sea urchin sperm tails (16). It is possible that twists are associated with bend propagation and therefore not revealed in this study.

The definitive, spontaneous sliding disruption of the axoneme in conjunction with structural markers in the axoneme and knowledge that the basal bend is the principal bend (2, 12, 19, 20, 22) has permitted determination of the relationship of axonemal organization to bending direction. High resolution darkfield light microscopy revealed that the larger set, subset 1, is located at the inside edge of the principal bend and the smaller set, subset 2, slides proximally on the convex, peripheral edge of the bend (Figs. 1 and 2). Subset 1 contains doublets 8, 9, 1, 2, 3 (or sometimes "8-4") and the central

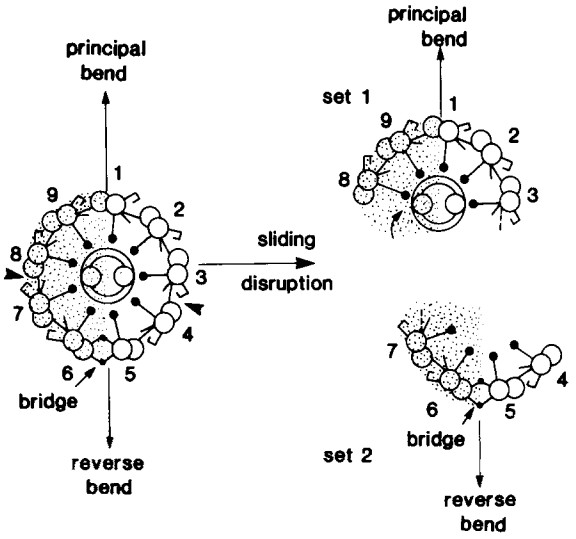

Figure 8. Summary illustration of the axis of the axoneme relative to the bending plane and direction. The bending plane bisects the central microtubule pair and passes through doublets 1 and between 5 and 6 (*arrows*). Furthermore, given that microtubule subset 1 is toward the inside edge of the principal bend (based on darkfield observations and longitudinal sections of bends) then doublet 1 leads the inside edge of the principal bend. Therefore, the 5-6 bridge sits in the leading edge of the axoneme for the reverse bend. *b* shows the typical pattern of axonemal fracture due to sliding apart of subsets 1 and 2 and illustrates the maintenance of structural organization of isolated subsets 1 and 2. The stippled regions define the components predicted to actively generate the basal principal bend. (Fig. 8 *a*, after Fig. 6 in reference 47).

pair (Figs. 7 and 8; Table III). Therefore, based upon the constant orientation of the central pair and the definitive pattern of microtubule sliding relative to the uniform, planar principal bend, doublet 1 is the inside edge of the principal bend. The 5-6 bridge is therefore the inside edge of the reverse bend (Fig. 8). Mohri et al. (26), using a different structural approach, determined that doublet 1 is the inside edge of the principal bend in starfish sperm.

These conclusions for the sea urchin sperm have depended upon: the enantiomorphic structure of the axoneme; the Ca^{2+}-induced uniform and stationary principal bend; the identification, by high resolution darkfield light microscopy, of the inside and outside edges of the principal bend with subset 1 and subset 2, respectively; and the maintenance of structural relationships of the central pair, 5-6 bridge, and doublets of both intact and fractured axonemes. Of potential functional significance is the observation that the microtubules of isolated subset 2 are maintained in a semi-circle configuration (Fig. 7). Therefore, spoke–central pair interaction is not required for maintenance of the circular profile. The arch-like arrangement of the subset 2 may contribute to the maintenance of planarity and lack of torsion of subset 2 during active extrusion. (In experiments not reported here we have observed the dramatic helical coiling of doublet subsets after exposure to proteases and glutaraldehyde as described earlier. See references 25 and 48.)

The axonemal axis described here for sea urchin sperm is virtually identical to that of cilia in the lateral epithelial cells of molluscan gills (13, 38). However, in sea urchin sperm the 5-6 bridge is the inside edge of the reverse bend direction,

whereas in the epithelial cilia the 5-6 bridge is the inside edge of the effective bend direction. Furthermore, Ca^{2+}-induced arrest of sea urchin sperm tails results in a trapping of the axoneme at the end of the principal bend with doublet 1 on the inside edge of the bend. Similarly, the Ca^{2+}-induced arrest of cilia of the lateral cells results in the trapping of cilia at the end of the reverse bend with doublet 1 at the inside edge (47). Therefore, relative to the axis and asymmetry of the axoneme, calcium stops the sperm tails and the lateral cell cilia in the same bend position with doublet 1 at the inside edge of the axoneme. This observation suggests a similar mechanism by which Ca^{2+} effects arrest for both the flagellum and cilium.

The axonemal axis of sea urchin sperm flagella can also be compared to the axis in *Chlamydomonas* flagella axonemes. The axoneme from *Chlamydomonas* flagella contains a "1-2 bridge" which is located at the inside edge of the reverse bend (23). Similarly, the 5-6 bridge of the sea urchin sperm tail is located at the inside edge of its reverse bend.

Formation of the Basal Principal Bend

As proposed by Gibbons and Gibbons (12) it is likely that the characteristic sharp stationary basal principal bend is a consequence of Ca^{2+}-induced asymmetry of active dynein cross-bridges around the 9 + 2 axoneme. Evidently Ca^{2+} and appropriate axonemal structures, possibly the radial spokes (see references 7 and 41, and further discussion below), induce a relaxed state in dynein arms responsible for reverse bend formation. (We have not addressed directly the molecular mechanisms through which Ca^{2+}-induced asymmetry of bending and quiescence are attained. The biochemical pathway may involve $CaATP^{2-}$ and asymmetrically distributed ATPases [28], calmodulin [8, 33], or alteration of phosphoproteins [41, 43, 46].) Presumably, dynein arms on doublets of one side of the axonemal axis generate unidirectional shear forces that accumulate at the basal body and result in a corresponding unidirectional bend. Consistent with this proposal for stationary basal bend formation is that isolated segments of axonemes missing the basal body cannot generate the Ca^{2+}-induced sharp basal bend and do not undergo the definitive, spontaneous sliding disruption described in this paper.

Based on the axis of the axoneme described here and the presumed unidirectional polarity of active microtubule sliding, we can predict the doublet microtubules which actively slide in the formation of the basal principal bend, and therefore we can suggest which doublets contain Ca^{2+}-relaxed dynein cross-bridges. Under the standard conditions of demembranation and reactivation described in Materials and Methods, subset 2 always slides proximally relative to subset 1. Based on the assumption that all dynein arms generate force with the same polarity such that they "push" the adjacent doublet tipward (37), subset 2 must slide in the proximal direction by the activity of the dynein arms of doublet 7: that is subset 2 "walks" as a group along doublet 8 of subset 1. Since the subset 2 loop never actively slides in the reverse direction under our standard conditions we assume that the dynein arms of doublet 3 of subset 1 (or doublet 4 when subset 1 is comprised of doublets 8-4) are functionally quiescent. Therefore, based on identification of the axis of the axoneme (Fig. 8) and the unidirectional polarity of active sliding, we predict that the activity of doublets on the 6-9 slide of the axoneme (stippled area, Fig. 8) are generally responsible for the formation of the basal principal bend. This implies that calcium causes the dynein arms of doublets 1-4 to be relatively inactive or relaxed, unable to generate a reverse bend. The observation that the basal bend is maintained through most of the transit period and only relaxes near the termination of subset 2 sliding (Fig. 2) confirms that part of the forces that generate the bend are the sliding forces that propel subset 2. Buffer conditions have not been defined which would result in stationary reverse bends. The proposal that the basal bend is generated by doublets on the 6-9 side of the axoneme is consistent with a radial switching model of regulation of active sliding (39).

Certain observations in this paper are not completely consistent with a simple radial switching model of basal bend formation. After sliding and separation of subsets, subset 1 only partially relaxes and a substantial portion of the principal bend is retained (Figs. 1, *c–e* and 2*a*). Therefore, factors other than the active cross-bridges of subset 2 contribute to the residual principal bend of subset 1. In other studies, it has been shown that high concentrations of vanadate (~millimolar) are required for reduced curvature of the stationary principal bend (12, 28), and that in the presence of vanadate and ATP, Ca^{2+} generates a further increase in principal bend curvature (28). Therefore, it is likely that the residual curvature of principal bend of subset 1 is maintained by active forces and that those forces are different from those that reside between subsets 1 and 2 before breakage.

It is also not clear why isolated subsets 1 and 2 do not bend or twist out of the original bend plane. If it is assumed that active cross-bridges are evenly distributed on doublets 6, 7, 8, and 9, then the isolated subset 1 should continue to contain active arms on doublets 8 and 9. Based on a simple switching model, the active arms of doublets 8 and 9 should, assuming passive sliding of doublets 1 and 2, generate a bend or twist out of the original plane toward doublet 3 in the plane of the central pair. Such twists or deviations from the original bend plane are not found. A similar question can be asked about the isolated subset 2. Presumably the arms of doublet 6 remain active and those of doublet 4 quiescent. It would, therefore, be expected that subset 2 should bend or twist out of the original plane. Such twists do occur (see Fig. 1*d*), however, if the completely detached subset 2 deviations from the original bend plane are not detected (Fig. 1*e*). Presumably the central pair, 5-6 bridge, and other components partially impede twists or bends. Alternatively, regions of active cross-bridges may not be evenly distributed between doublets 6-9 (see below).

To this point, discussion has focused on the relationship of these data to a radial switching model of basal bending in the axoneme. I can also partially address the issue of longitudinal localization of regions of active sliding. The patterns of active breakage described in Fig. 1*f* and 2*b* result from active shear at only a small region of contact (<5 μm), site x, between subsets 1 and 2. These observations demonstrate that only a limited longitudinal segment of active cross-bridges, on doublet 7, is sufficient to maintain the basal bend in subset 1 and overcome elastic and active forces which resist bending. That the principal bend of subset 1 is bent and compressed by a restricted region of cross-bridge activity is supported by the observations of repetitive separation of subsets 1 and 2 at site x followed by straightening of the axoneme, re-annealing of

subsets 1 and 2, and renewed unipolar sliding at the same region, site x, concurrent with renewed basal bending of subset 1. (With experimental measurement of the bending resistance of subset 1 [see Okuno, reference 27] it would be possible to calculate the sliding force in the region of contact at site x necessary to generate and maintain the basal bend.) The generation of the basal bend by active sliding at site x is consistent with other experiments that suggest local microtubule sliding is the basis for bending (see Shingyoji et al. [42]). Furthermore, as subset 2 is extruded, the sliding velocity appears to be relatively constant. Presumably, the number of dynein arms responsible for sliding decrease as subsets 1 and 2 separate. Since sliding velocity apparently does not decrease, then either elastic resistance to extrusion of subset 2 decreases proportionally to the decrease in the number of active dynein cross-bridges or active cross-bridges only exist at site x, and elastic resistance to sliding, after extrusion begins, is negligible.

It is not immediately apparent that the dynein arms of each doublet 6-9 are equally active in generating the basal principal bend of the Ca^{++}-induced sperm tails since the fracture is always restricted to a site between a pair of doublets on the 6-9 side of axoneme. However, we do find variations in the site of fracture. The predominant site is between doublets 7 and 8 but we also find fractures between doublets 6 and 7 and, to a more limited extent, between doublets 8 and 9 (Table III). Therefore, to various degrees, the arms of doublets 6, 7, and 8 are active, in extrusion of subset 2. It is possible that the frequency of the site of fracture on the 6-9 side of the axoneme reflects the degree of cross-bridge activity between pairs of doublets. However, as discussed below, the site of fracture most likely reflects the site of greatest stress due to greatest interdoublet sliding during basal bend formation.

It is reasonable that the point of minimal radius of curvature of the basal bend is a site of great outward stress. It is predictable that doublets located on the outer surface of the sharp bend, doublets 4, 5, 6, and 7, tend toward splitting away from the axoneme at the point of greatest curvature. The region of curvature contains site x (Fig. 1): the approximate point of initial separation of subsets 1 and 2. Furthermore, as illustrated in Table III and Scheme I, subset 2 is usually comprised of doublets that are symmetrically balanced around the bending axis, in particular doublets 4-7. If it is assumed that active cross-bridges are evenly distributed between doublets 6, 7, 8, and 9 on the active side of the axoneme and that interdoublet elastic links (nexin) are evenly distributed between all doublets, then we can predict, based on the axis described in this paper, that a planar bend would be expected to generate greatest interdoublet sliding between doublets 3 and 4 and 7 and 8; doublet pairs that are oriented parallel to the bending plane and the predominant sites of fracture. We predict that these points of greatest interdoublet sliding would be initial sites of fracture of nexin interdoublet links. Fracture of one nexin leads to fracture of the next, finally leading to sliding and relief of stress (see also discussion in reference 12). In effect, initial breakage of nexin links would result in planes of lowest resistance to sliding. No further disruption need take place upon relief of stress. (In many cases subset 2 is comprised of doublets 5-7. This combination of doublets is not symmetrical around the presumed bending axis. It is possible in these cases that the bend plane is actually skewed through doublet 6 or that the site of fracture on the 1-4 side of the axoneme is random.)

Endogenous proteolytic activity may be required for spontaneous breakage. Chick ovoinhibitor partially blocks the sliding disruption, and elastase treatment, under standard buffer conditions, promotes a similar pattern of sliding disruption. The limited pattern of disruption observed may be due to restricted sites of proteolysis under the conditions used (for further discussion see reference 45). However, it is more likely that elastase-like enzymes disrupt various axonemal sites randomly, perhaps including the nexin interdoublet links (see reference 3), and the restricted pattern of fracture reflects a combination of restricted pattern of active dynein cross-bridges and points of great mechanical stress as discussed above. This hypothesis is supported by the observation that the pattern of disruption is somewhat variable, therefore, active arms on doublets 6, 7, or 8 can effect proximal sliding of subset 2. Further it is unlikely that dynein arms of other doublets on the 1-4 side of the axoneme have in some way been permanently impaired, but rather are quiescent, since motility for intact axonemes can be restored by lowering the $MgATP^{2-}$ concentration (12, 34) and since random attachment of axonemes to the substrate can induced further random unrestricted sliding disruption (see Fig. 3).

The Role of the Radial Spoke System

Brokaw et al. (7) have concluded that the radial spoke system is primarily involved in inhibition of development of large curvature of reverse bends, therefore resulting in the normal asymmetric beating patterns of *Chlamydomonas* flagella. The results of this paper are consistent with such a proposal for the radial spoke system. Subset 1 maintains spoke–central pair attachments and also contains the doublets, numbers 1, 2, and 3, which we predict are involved in generating reverse bends. Therefore, we can speculate that through the action of Ca^{2+}, the radial spoke system has, through an undetermined mechanism, restricted curvature formation of reverse bends. Complete inhibition of development of reverse bend curvature could, therefore, result in a quiescent flagella with a stationary, basal principal bend. Further study of the functional and chemical properties of isolated subset 1 vs. subset 2 may reveal details of the mechanism of the radial spoke–central pair system.

I am grateful to Laura Ann Fox for excellent technical assistance and to Winifred Scherer for preparing the manuscript.

This work was supported by National Science Foundation Grant PCM-8119097 and National Institutes of Health RCDA HD 00553 and Grant HD 20497.

Received for publication 16 December 1985, and in revised form 21 February 1986.

References

1. Afzelius, B. 1959. Electron microscopy of the sperm tail: results obtained with a new fixative. *J. Biophys. Biochem. Cytol.* 5:269–278.
2. Brokaw, C. J. 1979. Calcium-induced asymmetrical beating of Triton-demembranated sea urchin sperm flagella. *J. Cell Biol.* 82:401–411.
3. Brokaw, C. J. 1980. Elastase digestion of demembranated sperm flagella. *Science (Wash. DC).* 208:1365–1367.
4. Brokaw, C. J. 1985. Cyclic AMP-dependent activation of sea urchin and tunicate sperm motility. *Ann. NY Acad. Sci.* 438:132–141.
5. Brokaw, C. J. 1986. Sperm motility. *Methods Cell Biol.* 27. In press.
6. Brokaw, C. J., R. Josslin, and L. Brobrow. 1974. Calcium ion regulation of flagellar beat symmetry in reactivated sea urchin spermatozoa. *Biochem. Biophys. Res. Commun.* 58:795–800.

7. Brokaw, C. J., D. J. L. Luck, and B. Huang. 1982. Analysis of movement of *Chlamydomonas* flagella: the function of the radial-spoke system is revealed by comparison of wild-type and mutant flagella. *J. Cell Biol.* 92:722–732.

8. Brokaw, C. J., and S. M. Nagayama. 1985. Modulation of the asymmetry of sea urchin sperm flagellar bending by calmodulin. *J. Cell Biol.* 100:1875–1883.

9. Gibbons, B. H. 1980. Intermittent swimming in live sea urchin sperm. *J. Cell Biol.* 84:1–12.

10. Gibbons, B. H. 1982. Reactivation of sperm flagella. *Methods Cell Biol.* 25:253–271.

11. Gibbons, B. H. 1982. Effects of organic solvents on flagellar asymmetry and quiescence in sea urchin sperm. *J. Cell Sci.* 54:115–135.

12. Gibbons, B. H., and I. R. Gibbons. 1980. Calcium-induced quiescence in reactivated sea urchin sperm. *J. Cell Biol.* 84:13–27.

13. Gibbons, I. R. 1961. The relationship between the fine structure and direction of beat in gill cilia of a lamellibranch mollusc. *J. Biophys. Biochem. Cytol.* 11:179–205.

14. Gibbons, I. R. 1961. Structural asymmetry in cilia and flagella. *Nature (Lond.).* 190:1128–1129.

15. Gibbons, I. R. 1963. A method for obtaining serial sections of known orientation from single spermatozoa. *J. Cell Biol.* 16:626–629.

16. Gibbons, I. R. 1975. The molecular basis of flagellar motility in sea urchin spermatozoa. *In* Molecules and Cell Movement. S. Inoue and R. E. Stephens, editors. Raven Press, NY. 207–231.

17. Gibbons, I. R. 1981. Cilia and flagella of eukaryotes. *J. Cell Biol.* 91(3, Pt. 2):107S–124S.

18. Gibbons, I. R. 1981. Transient flagellar waveforms during intermittent swimming in sea urchin sperm. II. Analysis of tubule sliding. *J. Muscle Res. Cell Motil.* 2:83–130.

19. Gibbons, I. R., and B. H. Gibbons. 1981. Transient flagellar waveforms during intermittent swimming in sea urchin sperm. I. Wave parameters. *J. Muscle Res. Cell Motil.* 1:31–59.

20. Goldstein, S. F. 1976. Form of developing bends in reactivated sperm flagella. *J. Exp. Biol.* 64:173–184.

21. Goldstein, S. F. 1977. Asymmetric waveforms in echinoderm sperm flagella. *J. Exp. Biol.* 71:157–170.

22. Goldstein, S. F. 1979. Starting transients in sea urchin sperm flagella. *J. Cell Biol.* 80:61–68.

23. Hoops, H. J., and G. B. Witman. 1983. Outer doublet heterogeneity reveals structural polarity related to beat direction in *Chlamydomonas* flagella. *J. Cell Biol.* 97:902–908.

24. Kamiya, R., R. Nagai, and S. Nakamura. 1982. Rotation of the central pair microtubules in *Chlamydomonas* flagella. *In* Biological Functions of Microtubules and Related Structures. H. Sakai, H. Mohri, and G. G. Borisy, editors. Academic Press, Inc., NY. 189–198.

25. Miki-Noumura, T., and R. Kamiya. 1979. Conformational change in the outer doublet microtubules from sea urchin sperm flagella. *J. Cell Biol.* 81:355–360.

26. Mohri, H., T. Mohri, and M. Okuno. 1985. Relationship between axonemal arrangement and bend direction in starfish spermatozoa. *Cell Motil.* 5:173.

27. Okuno, M. 1980. Inhibition and relaxation of sea urchin sperm flagella by vanadate. *J. Cell Biol.* 85:712–725.

28. Okuno, M., and C. J. Brokaw. 1981. Calcium-induced change in form of demembranated sea urchin sperm flagella immobilized by vanadate. *Cell Motil.* 1:363–370.

29. Okuno, M., and C. J. Brokaw. 1981. Effects of Triton extraction conditions on beat symmetry of sea urchin sperm flagella. *Cell Motil.* 1:363–370.

30. Olsen, G. E., and R. W. Linck. 1977. Observations on the structural components of flagellar axonemes and central pair microtubules from rat sperm. *J. Ultrastruct. Res.* 61:21–43.

31. Omoto, C. K., and C. J. Brokaw. 1983. Quantitative analysis of axonemal bends and twists in the quiescent state of Cionia sperm flagella. *Cell Motil.* 3:247–259.

32. Omoto, C. K., and C. Kung. 1980. Rotation and twist of the central-pair microtubules in the cilia of *Paramecium*. *J. Cell Biol.* 87:33–46.

33. Reed, W., S. Lebduska, and P. Satir. 1982. Effects of trifluoperazine upon the calcium-dependent ciliary arrest response of freshwater mussel gill lateral cells. *Cell Motil.* 2:405–427.

34. Sale, W. S. 1985. Study of the properties of $MgATP^{2-}$-induced stationary bends in demembranated sea urchin sperm. *Cell Motil.* 5:209–224.

35. Sale, W. S. 1985. A restricted pattern of active microtubule sliding disruption reveals that axonemal axis relative to bends in sea urchin sperm tails. *J. Cell Biol.* 101(5, Pt. 2):268a. (Abstr.)

36. Sale, W. S., U. W. Goodenough, and J. E. Heuser. 1985. The substructure of isolated and in situ outer dynein arms of sea urchin sperm flagella. *J. Cell Biol.* 101:1400–1412.

37. Sale, W. S., and P. Satir. 1977. Direction active microtubule sliding of microtubules in *Tetrahymena* cilia. *Proc. Natl. Acad. Sci. USA.* 74:2045–2049.

38. Satir, P. 1968. Studies on cilia. III. Further studies on the cilium tip and a "sliding filament" model of ciliary motility. *J. Cell Biol.* 39:77–94.

39. Satir, P. 1985. Switching mechanisms in the control of ciliary motility. *In* Modern Cell Biology. B. Satir, editor. Alan R. Liss, Inc., NY. 1–46.

40. Satir, P., and W. S. Sale. 1977. Tails of Tetrahymena. *J. Protozool.* 24:498–501.

41. Segal, R. A., and D. J. Luck. 1985. Phosphorylation in isolated *Chlamydomonas* axonemes: a phosphoprotein may mediate the Ca^{2+}-dependent photophobic response. *J. Cell Biol.* 101:1702–1712.

42. Shingyoji, C., A. Murakami, and K. Takahashi. 1977. Local reactivation of Triton-extracted flagella by iontophoretic applications of ATP. *Nature (Lond.).* 265:269–270.

43. Stommel, E. W., and R. E. Stephens. 1986. Cyclic AMP and calcium in the differential control *Mytilus* gill cilia. *J. Comp. Physiol.* In press.

44. Sugino, K., and Y. Naitoh. 1982. Simulated cross-bridge patterns corresponding to ciliary beating in Paramecium. *Nature (Lond.).* 295:609–611.

45. Tamm, S. L., and S. Tamm. 1984. Alternate patterns of doublet microbutule sliding in ATP-disintegrated macrocilia of the ctenophore *Beroë*. *J. Cell Biol.* 99:1364–1371.

46. Tash, J. S., P. Kelly, and A. R. Means. 1982. Identification of calmodulin-dependent pathways in the regulation of dog sperm function. *J. Cell Biol.* 101(5, Pt. 2):2670. (Abstr.)

47. Wais-Steider, J., and P. Satir. 1979. Effect of vanadate on gill cilia: switching mechanism in ciliary beat. *J. Supramol. Struct.* 11:339–347.

48. Zobel, C. R. 1973. Effect of solution composition and proteolysis on the conformation of axonemal components. *J. Cell Biol.* 59:573–594.